

# Coupling of discrete-element method and smoothed particle hydrodynamics for liquid-solid flows

Yrjö Jun Huang<sup>a)</sup> and Ole Jørgen Nydal

*Department of Energy and Process Engineering, Norwegian University of Science and Technology (NTNU), Trondheim, Norway*

(Received 10 September 2011; accepted 27 September 2011; published online 10 January 2012)

**Abstract** Particle based methods can be used for both the simulations of solid and fluid phases in multiphase medium, such as the discrete-element method for solid phase and the smoothed particle hydrodynamics for fluid phase. This paper presents a computational method combining these two methods for solid-liquid medium. The two phases are coupled by using an improved model from a reported Lagrangian-Eulerian method. The technique is verified by simulating liquid-solid flows in a two-dimensional lid-driven cavity. © 2012 The Chinese Society of Theoretical and Applied Mechanics. [doi:10.1063/2.1201202]

**Keywords** discrete-element method, smoothed particle hydrodynamics, liquid-solid flows, lid-driven cavity

Mesh generation is a time-consuming task in computational simulation. Mesh free methods abandon this concept. Several meshless methods have been developed for fluid mechanics since 1970s. Among all these methods, smoothed particle hydrodynamics (SPH) is one of the earliest methods. It was developed for solving astro-physical problems.<sup>1,2</sup> Later it was also used for the simulations of different types of fluid flows, because the movement of particles in astrophysical flows is similar to those in liquid or gas flows. The idea of the SPH method is building a set of disordered particles in a continuum without grid or mesh. Each particle has an associated mass, momentum and energy. The motion of the particle is calculated from the integration of Newton's second law. A property for each particle within the flow, such as density, is obtained from an interpolation of the neighboring particles by using the following approximate averaging operator, which is also called kernel function<sup>3,4</sup>

$$f(x_i) = \int_{\Omega} f(x')\delta(x - x')dx' \approx \sum_{j=1}^N f(x_j)W(x_i - x_j, h)V_j, \quad (1)$$

where  $\delta$  is the Dirac delta function,  $W$  is the smoothing kernel function and  $h$  is the smoothing length defined the influence area of  $W$ ,  $V_j$  is the space occupied by the  $j$ th particle,  $\Omega$  is the space of the integral which contains  $x$ , also called support domain and  $N$  is the number of discrete particles in  $\Omega$ .

Also in 1970s, Cundall developed discrete-element method (DEM) for the analysis of rock-mechanics problems<sup>5</sup> and then this method was applied to soils.<sup>6</sup> Same as that in SPH, the motion of each particle in DEM is also described by the Newton's law, that the sum of all forces acting on it is intergraded over tiny

time steps to find the particle's velocity and position. Comparing with the Eulerian methods for particulate flows, we can easily capture the key features and details of the system to provide details which are helpful in the development of accurate models.<sup>7,8</sup> Hence, the DEM algorithm looks similar to SPH because both of them are numerically intergraded subjected to forces applied by the neighboring particles. The major difference is that the inter-particle forces in SPH are derived from the Navier-Stokes equations and those forces in DEM are due to particle contact process.<sup>9</sup>

A lot of researches using DEM to couple with mesh-based computational fluid dynamics (CFD) technique, namely Lagrangian (particle-based) and Eulerian (mesh-based) methods (La/Eu), to simulate the liquid-solid flows have been carried out.<sup>10,11</sup> The volume fraction,  $\phi$ , is an important parameter for coupling the phases in these simulations, because the drag force is described as a function of  $\phi$ .<sup>10,12</sup> These researches cannot get rid of the mesh generation process in the simulations thoroughly. Ten years ago, Potapov et al.<sup>13</sup> showed some simulations of coupling of the SPH and DEM methods, which is different from the other previous approaches for liquid-solid flows. The size of the solid beads in the system are much larger than the inter-particle spacing for the fluid SPH particles in their simulations. No-slip boundary conditions were applied to couple the fluid particles close to the solid surface and those solid particles composed the beads surface. Recently, Huang et al.<sup>14</sup> showed their SPH simulations using multi-mass particles. This technique makes it easy to combine the SPH and DEM methods for the solid-fluid problems with tiny beads.

This paper presents some results of an ongoing study of solid-liquid flow with tiny solid beads by combining SPH and DEM. It is a Lagrangian-Lagrangian (La/La) method and no mesh is required more.

Each particle carries individual mass and occupies individual space in SPH method for single phase. The density of the  $i$ th particle,  $\rho_i$ , in a particulate sys-

<sup>a)</sup>Corresponding author. Email: jun.huang@ntnu.no.

tem can be evaluated by using the summation density approach<sup>4,15</sup>

$$\rho_i = \sum_{j=1}^N m_j W_{i,j} / \sum_{j=1}^N \left( \frac{m_j}{\rho_j} \right) W_{i,j}, \quad (2)$$

where  $\rho_j$  is the density and  $m_j$  is the mass of the  $j$ th particle of the  $N$  fluid particles supporting domain. It is well suited for the normalization condition and strictly ensures the conservation of mass. We have adopted this approach in this paper.

Based on the summation density approach, the mass conservation equation and the momentum equation also can be written in particle form as<sup>16,17</sup>

$$\frac{d\rho_i^{x_1}}{dt} = \rho_i \sum_{j=1}^N \frac{m_j \mathbf{v}_{ij}}{\rho_j} \frac{\partial W_{ij}}{\partial \mathbf{x}_i^{x_2}}, \quad (3)$$

and

$$\rho_i \frac{d\mathbf{v}_i^{x_1}}{dt} = \sum_{j=1}^N \frac{m_j \boldsymbol{\sigma}_j^{x_1, x_2}}{\rho_j} \frac{\partial W_{ij}}{\partial \mathbf{x}_i^{x_2}}, \quad (4)$$

where  $\mathbf{v}$  is velocity,  $t$  is time,  $\boldsymbol{\sigma}$  is stress tensor and  $\mathbf{x}$  is coordinate in the kernel function. The stress tensor is made up of two parts, the isotropic pressure and the viscous stress. If external forces are considered, the momentum equation Eq. (4) becomes

$$\rho_i \frac{d\mathbf{v}_i^{x_1}}{dt} = \sum_{j=1}^N \frac{m_j \boldsymbol{\sigma}_j^{x_1, x_2}}{\rho_j} \frac{\partial W_{ij}}{\partial \mathbf{x}_i^{x_2}} + \frac{\sum \mathbf{F}_{\text{ext}}}{V_i}. \quad (5)$$

The external forces include the gravitation and the solid-fluid interaction.

The motion of each solid bead in a solid-liquid system can be described by the Langevin equation, as

$$m \frac{d\mathbf{v}}{dt} = \mathbf{F}^i + \mathbf{F}^D + \mathbf{F}^b + \mathbf{F}^g. \quad (6)$$

where the four terms on the right hand side are due to bead-bead contact, drag force and buoyancy force from the fluid phase, and gravity force. To simplify the problems, the shapes of the beads are assumed to be spherical or spheroidal and each particle stands for a solid bead. A DEM algorithm given by Ramírez et al.<sup>18</sup> was chosen in our simulations, that the bead-bead contact process could be modeled as a spring-dashpot system. The normal interaction force is the sum of an elastic term and a viscous term

$$\mathbf{F}_n = \mathbf{F}_n^e + \mathbf{F}_n^d = K_n \delta_n^\zeta + \eta_n \delta_n^\xi \dot{\delta}_n, \quad (7)$$

where  $\zeta = 3/2$ ,<sup>19,20</sup>  $\xi = 0.5$  by dimensionless analysis,<sup>21</sup>  $\delta_n$  is the overlap,  $\delta_n = r_i + r_j - d_{ij}$  ( $\delta_n > 0$ ),  $K_n$  is the effective stiffness,  $\eta_n$  is the damping coefficient,  $r_{i,j}$  is the radius of each bead and  $d_{ij}$  is the distance between the two centers of the beads. While for a constant coefficient of restitution (COR) in the normal direction,  $e$ ,  $\zeta$  the details of other coefficients are described in Refs. 7, 22. The magnitude of tangential

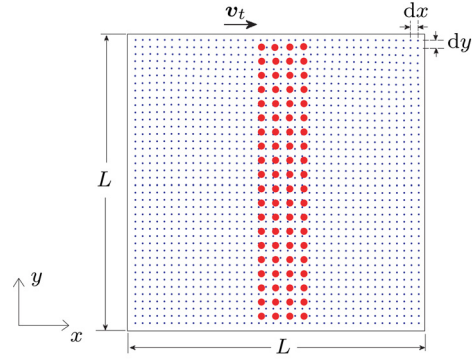


Fig. 1. Location of the particles in the lid-driven square cavity at  $t = 0$  s. The big dots for solid beads and the small dots are for fluid particles in the system. The initial velocities of all particles are zero. The origin of the  $xy$ -coordinate system is located in the lower-left corner of the cavity.

force,  $|\mathbf{F}_{t,i}|$ , is obtained from Coulomb's friction law that  $|\mathbf{F}_{t,i}| = \mu |\mathbf{F}_{n,i}|$ . In the simulations shown in this paper,  $e = 0.9$  and  $\mu = 0$  were selected.

The drag force term in Eq. (6) presents the force on solid beads due to the velocity relative to the surrounding fluids. For a single spherical bead, it can be written as<sup>12</sup>

$$\mathbf{F}_s^D = 3\pi d_s \rho_f \nu_f \phi_f^\beta (1 + 0.15 Re_p^{0.678}) (\mathbf{v}_f - \mathbf{v}_s), \quad (8)$$

where  $Re_p$  is the particle Reynolds number,  $Re_p = \phi_f d_s |\mathbf{v}_f - \mathbf{v}_s| / \nu_f$ ,  $d_s$  is the diameter of the solid bead,  $\rho_f$  is the density,  $\nu_f$  is the viscosity of the fluids, the exponent  $\beta$  varies with the particle Reynolds number, the subscripts s and f are for solid and fluid particles respectively. In our simulations, the density  $\rho_f$  is obtained by from Eq. (2) and the velocity of the surrounding fluids for the solid particle  $i$ ,  $\mathbf{v}_{f,i}$  is approached by averaging the surrounding fluid particles

$$\mathbf{v}_{i,f} = \sum_{j=1}^N \mathbf{v}_j m_j / \sum_{j=1}^N m_j \quad (9)$$

The buoyancy force term is given by

$$\mathbf{F}_s^b = (\rho_f - \rho_s) V_s \cdot \mathbf{k}, \quad (10)$$

where  $\mathbf{k}$  is the unit vector paralleling with gravitation.

The aforementioned drag force and the buoyancy force act on the solid beads, then the equal and opposite forces should be acted upon the fluid particles. Employing the kernel function, we approach these reactions on each fluid particle by

$$\mathbf{F}_{f,k}^{D,b} = \mathbf{F}_s^{D,b} \cdot (V_{f,k} W_{k,j}) / \sum_{j=1}^N V_{f,j} W_{i,j}. \quad (11)$$

Adding the fluid-solid interaction to the momentum equation for fluid phase, we find that Eq. (5) becomes

$$\rho_{f,i} \frac{d\mathbf{v}_{f,i}^{x_1}}{dt} = \sum_{j=1}^N \frac{m_{f,j} \boldsymbol{\sigma}_j^{x_1, x_2}}{\rho_{f,j}} \frac{\partial W_{ij}}{\partial \mathbf{x}_i^{x_2}} + \frac{\mathbf{F}_{f,i}^b + \mathbf{F}_{f,i}^D}{V_{f,i}}. \quad (12)$$

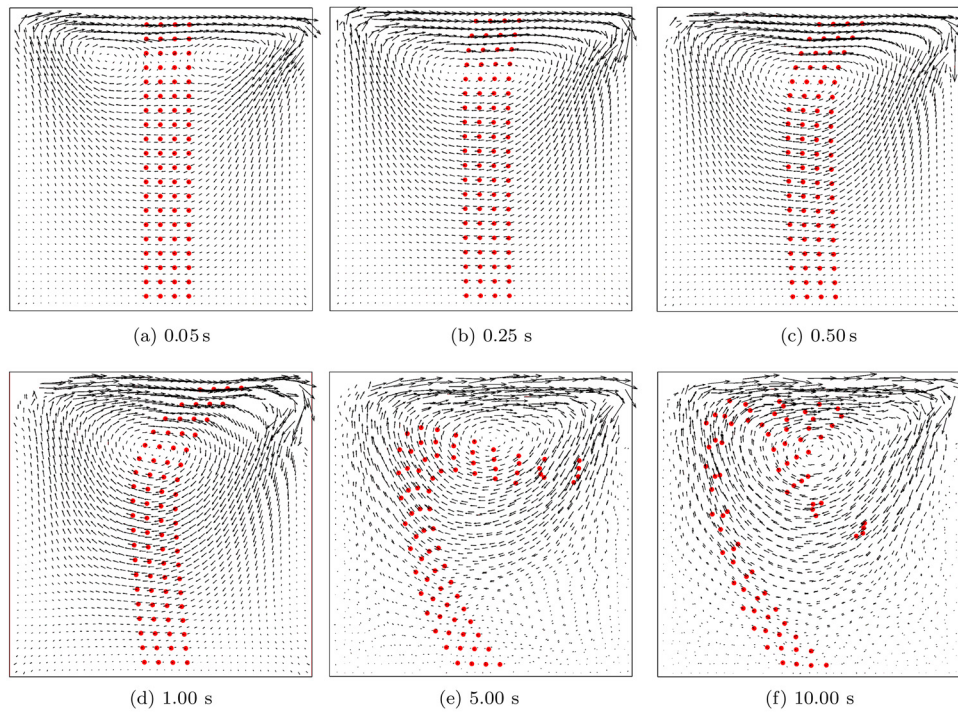


Fig. 2. Location and velocity profiles of the lid-driven square cavity at different times. Here, the solid dots are for the solid beads in the system.

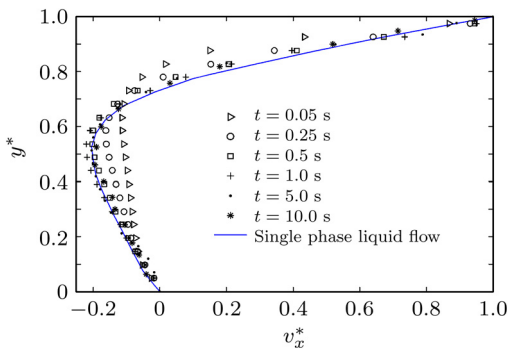


Fig. 3. Dimensionless velocity along the vertical central line of the cavity. The different types of dots are for the solid-fluid flows at different time. The curve is for a single-phase fluid flow with the same boundary conditions when it arrives steady state.

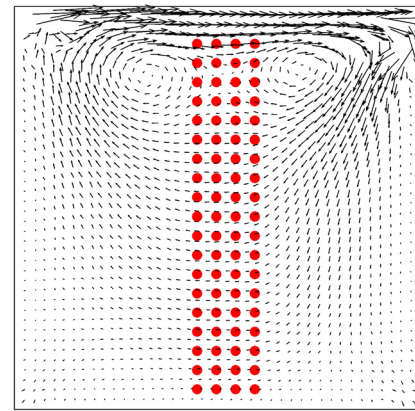


Fig. 4. The flow field of fixed and concentrated dense solid beads, which can be used for simulation of porous materials.

The lid-driven cavity flow is perceived as a textbook example and usually it is determined qualitatively in the simplest case of the flow in a two dimensional (2D) square cavity. The comparison with this classical phenomena has been used to examine the ability and efficiency of a simulation method.<sup>14,23–26</sup> A simulation of solid-liquid flow in a 2D lid-driven square cavity is presented. The simulation region consists of  $40 \times 40$  fluid particles and  $20 \times 4$  solid beads, with shear moving boundary conditions at the top side and bounce-back boundary conditions at the left, right and bottom sides. The diameter of these solid beads is 1 mm, the

density of the fluid phase is  $1\,000\text{ kg/m}^3$ , and the viscosity  $\nu_f = 1\,000\text{ m}^2/\text{s}$ . Gravitation is not considered in the simulations. The square simulational domain is sketched in Fig. 1 with side length  $L = 0.01\text{ m}$  and the velocity of the top boundary,  $\mathbf{v}_t$ , is  $0.01\text{ m/s}$ . The mass of each fluid particle is obtained by

$$m_{f,i} = \rho_{f,i} dx dy \cdot \sum_{j=1}^N V_{s,j} W_{i,j} / V_h, \quad (13)$$

where  $N$  is the number of solid particles in the  $i$ th particle's supporting domain and  $V_h$  is space of the supporting domain. For 2D problems,  $V_h = 3\pi h^2/4$ , where

$h$  is the radius of the supporting domain. It is reported that a prime eddy forms at  $0.24L$  below the lid in the mid-plane for water flow, when the Reynolds number is 100, where the Reynolds number  $Re = Lv_t/\nu$ .<sup>27</sup> Because gravitation is not considered in this simulation, the buoyancy force also approaches zero.

Figure 2 shows the transient behavior of the particles in the cavity. The snapshots are taken at six different times:  $t = 0.05$  s,  $0.25$  s,  $0.5$  s,  $1.0$  s,  $5.0$  s and  $10.0$  s. As shown in Fig. 2(a), the motion of the solid beads affects the flow field in the beginning. Because the motions of those solid beads are caused by the flow of the fluid phase, there exists a delay between the motions of these two phases. The quasi-static solid beads separate the cavity into two chambers and the fluid in each chamber forms an eddy. The flow field reaches a steady state gradually and the relative velocity between the two phases approaches to zero. With the movement of the solid beads, the two chambers connect to each other, and these two eddies combine to a prime one. Figures 2(a)–2(c) present this process. Each particle in the system is propagating along a closed streamline. To compare the velocity profiles, another SPH simulation for single-phase liquid flow in the same cavity was carried out. All the dimensionless velocities along the vertical central line ( $x = L/2$ ) at different times are plotted in Fig. 3, as well as the single-phase liquid flow at steady state. The dimensionless velocities and coordinate are defined as  $v_x^* = v_x/v_t$  and  $y^* = y/L$ , respectively. From Fig. 3, it also can be seen that the eddy center of the solid-liquid flow approaches that of the single-phase liquid flow after  $0.5$  s in our simulations.

On the other hand, if the mass of the solid particles were set as great enough, the two chambers shown in Fig. 2(a) become stable. The convection between the chambers becomes weak. The performance of the dense solid phase concentrated in the middle of the simulation domain is similar to porous materials. Figure 4 shows the flow field of  $t = 0.1$  s when the density of the solid phase is set as  $10^8$  kg/m<sup>3</sup>. All the aforementioned simulation results and theoretical explanations show the validation of the SPH-DEM coupling technique.

This paper presents a La/La algorithm to simulate solid-fluid phase flows. The motion of the solid phase is simulated by using DEM while the fluid aspect is simulated by using SPH. The coupling of the two aspects are followed from some solid-fluid interaction models for La-Eu methods. Employing this method, we find that the sizes of the solid beads are very flexible, namely from infinite to the same scale as the smooth length in the SPH aspect, which is helpful to control and balance the CPU time in the two aspects. The method is verified

by an example of solid-fluid flow in a square lid-driven cavity.

*The authors thank Prof. Liu Moubin of the Key Lab for Hydrodynamics and Ocean Engineering, Institute of Mechanics, Chinese Academy of Sciences for using their Codes.<sup>4</sup> This work was partially supported by Department of Energy and Process Engineering, Norwegian University of Science and Technology, Institute for Energy Technology and SINTEF through the FACE (Multiphase Flow Assurance Innovation Center) Project.*

1. L. B. Lucy, *Astronomical J.* **82**, 1013 (1977).
2. R. A. Gingold, and J. J. Monaghan, *Monthly Notices of Royal Astro. Soc.* **181**, 375 (1977).
3. S. Li, and W. K. Liu, *Appl. Mech. Rev.* **55**, 1 (2002).
4. G. R. Liu, and M. B. Liu, *Smoothed particle hydrodynamics, a meshfree particle method* (World Scientific 2003).
5. P. A. Cundall, *Proceeding of the Symposium of International Society of Rock Mechanics* (Nancy, France, 1971).
6. P. A. Cundall, and O. D. L. Strack, *Geotechnique* **29**, 47 (1979).
7. J. Huang, C. K. Chan, and P. Zamankhan, *Phys. Rev. E* **82**, 031307 (2010).
8. Y. J. Huang, and O. J. Nydal, *Communications in Computational Physics* **10**, 1027 (2011).
9. P. W. Cleary, and M. Prakash, *Phil. Trans. R. Soc. Lond. A* **362**, 2003 (2004).
10. Y. Tsuji, T. Kawaguchi, and T. Tanaka, *Power Technology* **77**, 78 (1993).
11. P. Zamankhan, J. Huang, and S. M. Mousavi, *J. Offshore & Arctic Eng.* **129**, 176 (2007).
12. C. Y. Wen, and Y. H. Yu, *Chem. Eng. Proc. Symp. Ser.* **62**, 100 (1966).
13. A. V. Potapov, M. L. Hunt, and C. S. Campbell, *Powder Tech.* **116**, 204 (2001).
14. Y. J. Huang, and O. J. Nydal, Particle refined and coarsened method for SPH simulations in fluid dynamics, <http://www.youtube.com/watch?v:ZH2Rwrmrko>.
15. P. W. Randles, and L. D. Libersky, *Compu. Methods in Appl. Mech. & Eng.* **139**, 375 (1996).
16. L. D. Libersky, A. G. Petscheck, and T. C. Carney, et al, *J. Compu. Phys.* **109** 67 (1993).
17. C. E. Zhou, G. R. Liu, and K. Y. Lou, *Int. J. Compu. Methods* **4** 671 (2007).
18. R. Ramirez, T. Poschel, and N. V. Brilliantov, et al, *Phys. Rev. E.* **60**, 4465 (1999).
19. H. Hertz, *J. Reine Angew. Math.* **92**, 156 (1882).
20. K. L. Johnson, *Contact Mechanics* (Cambridge Univ. Cambridge 1982).
21. G. Kuwabara, and K. Kono, *Jpn. J. Appl. Phys.* **26**, 1230 (1987).
22. R. D. Mindlin, *J. Appl. Mech.* **16**, 259 (1949).
23. S. Hou, Q. Zou, and S. Chen, et al, *J. Compu. Phys.* **118**, 329 (1995).
24. L. Larchevêque, P. Sagaut, and I. Mary, et al, *Phys. Fluids* **15**, 193 (2003).
25. T. Watanabe, and K. Ebihara, *Nuclear Eng. & Design* **188**, 111 (1999).
26. P. N. Shankar, and M. D. Deshpande, *Ann. Rev. Fluid Mech.* **32**, 93 (2000).
27. U. Ghia, K. N. Ghia, and C. T. Shin, *J. Compu. Phys.* **48**, 387 (1982).